Ultralow emittance electron beams from a laser-wakefield accelerator

R. Weingartner,[1,2] S. Raith,[1,2] A. Popp,[1,2] S. Chou,[1,2] J. Wenz,[1,2] K. Khrennikov,[1,2] M. Heigoldt,[1,2] A. R. Maier,[1,2] N. Kajumba,[1,2] M. Fuchs,[1,2] B. Zeitler,[3,1] F. Krausz,[1,2] S. Karsch,[1,2] and F. Grüner[3,1,*]

[1]*Department für Physik, Ludwig-Maximilians Universität, 85748 Garching, Germany*
[2]*Max-Planck Institut für Quantenoptik, 85748 Garching, Germany*
[3]*Institut für Experimentalphysik, Universität Hamburg, 22607 Hamburg, Germany*

(Received 8 February 2012; published 5 November 2012)

Using quadrupole scan measurements we show laser-wakefield accelerated electrons to have a normalized transverse emittance of $0.21^{+0.01}_{-0.02}\pi$ mm mrad at 245 MeV. We demonstrate a multishot and a single-shot method, the mean emittance values for both methods agree well. A simple model of the beam dynamics in the plasma density downramp at the accelerator exit matches the source size and divergence values inferred from the measurement. In the energy range of 245 to 300 MeV the normalized emittance remains constant.

DOI: 10.1103/PhysRevSTAB.15.111302 PACS numbers: 41.85.Ja, 29.27.Fh, 41.85.Lc, 52.38.Kd

Laser-wakefield acceleration (LWFA) [1,2] can deliver ultrarelativistic electron beams in a compact setup with unique features [3–6]. It is receiving particular attention as a source or driver for ultrashort x-ray beams [7,8] and for its potential for realizing a tabletop free-electron laser (FEL) [9]. The electron bunch duration has recently been measured to be only a few femtoseconds long [10,11] which results in peak beam currents on the order of kiloamperes. An essential parameter for the performance of x-ray sources, FELs, or linear colliders is the transverse electron beam emittance. Previous emittance measurements of LWFA electron beams have used the pepper-pot method [12–14] giving normalized emittances of $\sim 2.2\pi$ mm mrad with single shots down to the resolution limit of 1.1π mm mrad. As these measurements are not spectrally resolved, they rely on a low energy spread to give a meaningful normalized emittance. For LWFA beams which fluctuate in energy and energy spread, a simultaneous measurement of the spectrum is required. This technique is also limited to electron energies that can be sufficiently scattered by the pepper-pot mask; to date, measurements of a 508 MeV beam have been carried out [15]. Experiments characterizing the betatron radiation emitted by the electron beam while it is in the plasma suggest the beam size there to be $\lesssim 1$ μm [16,17], which in combination with a divergence measurement give an estimated emittance of $<0.5\pi$ mm mrad [18]. However, inferring the emittance from the electron beam size in the plasma and its downstream divergence in the vacuum can be unreliable as this neglects the plasma-vacuum density transition at the accelerator exit; here the decreasing strength of the plasma focusing forces result in an increase in beam size and decrease in divergence [13]. This publication reports on direct measurements of the emittance of LWFA electrons that are both energy resolved and that include the beam transport of the density downramp at the accelerator exit. This is achieved by analyzing their beam size around a focus using a quadrupole lens scan method [19].

The transverse phase space of an electron beam is often specified using the Twiss parameters α, β, γ, and the natural emittance ε. These parameters describe the volume and orientation of the particle distribution in phase space. The beam size at a particular position $\sigma(s_1)$ is related to the Twiss parameters at s_0 by [20]

$$\sigma(s_1)^2 = M_{11}^2 \epsilon \beta(s_0) - 2M_{11}M_{12}\epsilon\alpha(s_0) + M_{12}^2\epsilon\gamma(s_0). \quad (1)$$

Here M_{ij} refers to the ij element of the transport matrix which is the product of the drift and quadrupole matrices between s_0 and s_1. By measuring the beam size $\sigma(s_1)$ for various M, the Twiss parameters and the emittance are found using a least-squares fit algorithm. In a typical quadrupole scan measurement, M is varied by changing the quadrupole strength such that the beam passes through a focus at s_1 for the best accuracy. In our case the quadrupole strength is fixed so we vary the position of a lens, or measure $\sigma(s_1)$ for different beam energies.

The driver laser in our experiment, the ATLAS facility at the MPI of Quantum Optics, delivers 1.5 J pulses of 28 fs FWHM duration on target. The laser pulse is focused by an $f/22$ off-axis parabola into a hydrogen-filled gas cell (density 6×10^{-18} cm^{-3}) which typically produces electron beams that have a plateau spectrum with charge 0.2 pC/MeV up to an energy of $\sim$350 MeV. At this energy there is typically a peak on top of the plateau with 0.4 pC/MeV and an rms energy spread of 6% containing an integrated charge of 15 pC [21]. Because of the fluctuations in peak electron energy, the measurements were

*florian.gruener@physik.uni-muenchen.de

conducted slightly below the 350 MeV peak to ensure that sufficient charge was available for every shot. The electron beams are characterized with a scintillating screen (transverse profile), and a cerium-doped YAG crystal (diameter 10 mm, thickness 0.3 mm) behind a dipole magnet to observe the spectrally resolved beam size with a high spatial resolution (see Fig. 1). The observed electron energy depends on the position of the YAG crystal along the dispersion plane. At an energy of 300 MeV an energy range of ~4 MeV can be observed on a single shot. A permanent magnet quadrupole lens doublet can be inserted into the beam ~10 cm after the gas cell to focus the beam [22]. As the focal length of the lens system depends on the electron energy, the magnification is also a function of energy; in our setup we have magnifications of approximately 25 to 30. The imaging system observing the YAG crystal consists of an $f/2$ 50 mm aspherical achromat and an apochromatic Canon $f/2$ 135 mm camera objective both working at an infinite conjugate ratio. The measurement resolution is limited by the thickness of the YAG crystal and the resulting depth of field blurring. Therefore we used the thinnest crystal (0.3 mm) that still provided enough scintillation yield for a sufficient signal to noise ratio. The point spread function of the optics including the depth of field was determined empirically using an USAF 1951 resolution target and is well modeled by a Gaussian curve with an rms width of 3.5 μm. It is known that the resolution of YAG crystals deteriorates for high charge density electron beams [23]. However, this is only relevant for charge densities that are 3 orders of magnitude higher than those in our experiments. The magnetic field aberrations of the quadrupole lenses were minimized by carefully shifting their individual magnet wedges [24]. Simulations comparing the electron beam focus of perfect quadrupole lenses and the optimized lenses as used in the experiment show a discrepancy of ~1%. We therefore disregard the lens aberrations in our emittance analysis.

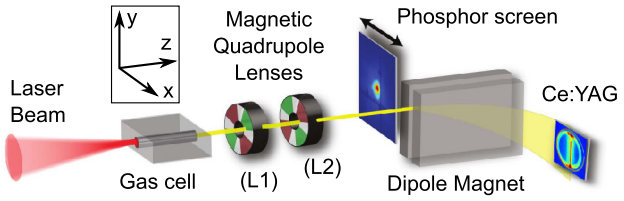

FIG. 1. A laser pulse is focused into a 5 mm long hydrogen-filled gas cell and accelerates electrons up to ~350 MeV. The electrons pass through a pair of magnetic quadrupole lenses ~10 cm behind the gas cell which focus the electron beam. The first lens is 25 mm long and the second lens 15 mm; both have a measured field gradient of ~480 T/m. The transverse profile of the beam is observed on a removable scintillating screen. A dipole magnet with field strength 1 T disperses the beam and allows the observation of the energy-resolved beam size of a few-MeV bandwidth on a high-resolution YAG crystal screen 2.16 m behind the gas cell.

Figure 2 shows a scan of the z position of lens two and the resulting measured beam size at the YAG crystal positioned behind the dipole magnet such that electrons with an energy of 245 MeV are observed. Each data point is the mean rms beam width of 15 or more shots; the width of each shot is evaluated for a small integrated energy bandwidth (~ 0.05 MeV) around the observed energy. The fit curve corresponds to a normalized emittance of $0.21^{+0.01}_{-0.02}\pi$ mm mrad with the resolution of the imaging optics taken into account; the limits are estimated by fitting through the upper and lower error bars (± 1 standard error of the mean). For 270 and 300 MeV electrons the measured normalized emittances are $0.17^{+0.02}_{-0.01}$ and $0.19^{+0.03}_{-0.01}\pi$ mm mrad, respectively, indicating a constant normalized emittance. This supports the expected linear focusing forces in the wakefield during acceleration as has been previously observed at lower electron energies of <20 MeV [13]. The effective rms source size and divergence at the gas cell exit are 0.93 μm and 0.45 mrad, respectively. The derived source divergence agrees well with the divergence determined by measuring the beam size after a free drift. Figure 2 also shows the effect of space charge on the measurement. To focus a beam

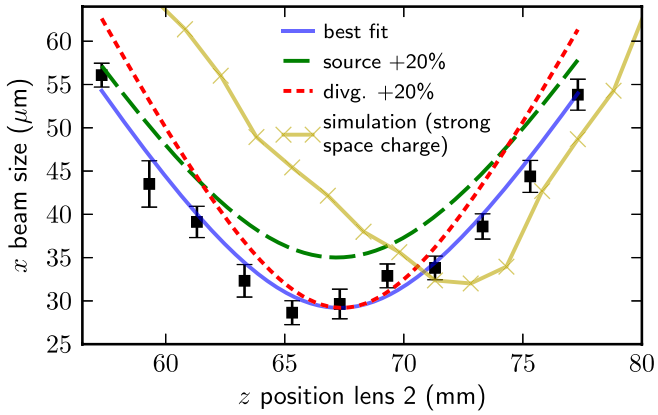

FIG. 2. Lens position scan for 245 MeV electrons. The mean rms beam sizes and their standard error are plotted against the z position of lens two (black squares). The fit curve (blue) neglects space charge and gives a normalized emittance of $0.21^{+0.01}_{-0.02}\pi$ mm mrad and inferred rms source size and divergence of 0.93 μm and 0.45 mrad, respectively. The accuracy of the method is illustrated by the expected dependence for a 20% larger emittance by increasing the inferred source size or divergence. The influence of space charge is shown by the yellow line; a particle tracking simulation [33] of 3000 macroparticles including point-to-point space charge for an initially monoenergetic 245 MeV, 50 pC beam with duration 4.5 fs shows a clear deviation from our measurements. The initial source size and divergence in the simulation were chosen to be 0.25 μm and 0.45 mrad, respectively, to obtain a similar curve as obtained from the measurements. Note the steeper flank on the right-hand side of the space charge curve. A tracking simulation without space charge matches the blue fit curve which confirms the extracted emittance value from the data.

including space charge requires a stronger focusing lens system to compensate the repulsion of the electrons. In our case stronger focusing is achieved by increasing the z position of lens two, resulting in the shift of the beam size curve as seen in Fig. 2. Furthermore, quadrupole scans of beams with significant space charge display an asymmetry about their minimum, with the stronger focusing side (larger lens two z position) showing a steeper flank [25]. As the measured data does not show a significant asymmetry or shift, space charge effects must be much less significant in the experiment than in the simulation in Fig. 2. As the charge is reduced in the simulation, the yellow curve moves towards the measured data, becomes symmetric, and eventually matches the blue fit curve. The measurement accuracy benefits from the spectral splitting of the beam behind the dipole magnet which reduces the charge density and hence the space charge repulsion of the beam. The measured data therefore confirms that space charge is negligible in our experiment.

An alternative way to obtain the emittance using Eq. (1) is to scan the beam energy as opposed to the position of a lens. In our experiment we can evaluate the beam size for the small range of energies (~ 4 MeV, see Fig. 3) observable on the YAG crystal for a single shot. The fit curve in the figure gives a normalized emittance of $0.14 \pm 0.01\pi$ mm mrad with an effective rms source size and rms divergence of 0.62 μm and 0.39 mrad, respectively. We compare the lens two z position scan to this single-shot method by averaging over several shots. For the 16 shots comprising the data point at 67 mm in Fig. 2 for 245 MeV electrons, the mean emittance is $0.21 \pm 0.08\pi$ mm mrad with an inferred source size and divergence of 0.95 μm and 0.44 mrad, respectively. Similarly for 270 and 300 MeV, the values of the two methods agree to within 10% of each other. Hence, the emittance values obtained here from the single-shot (energy-scan) method are consistent with the multishot (lens position scan) measurement results above.

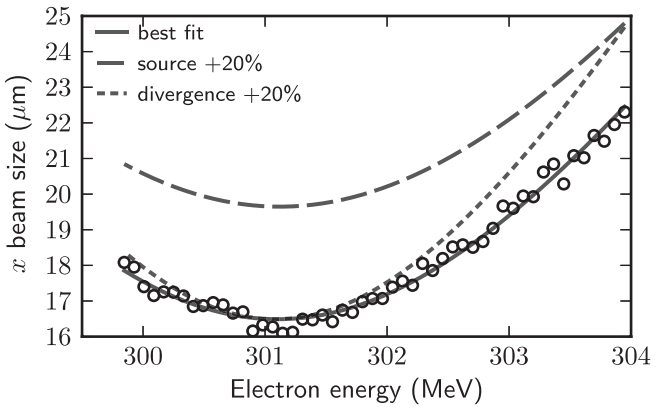

FIG. 3. The rms beam size vs beam energy for a single shot (circles). The solid fit line corresponds to a beam with normalized emittance of $0.14 \pm 0.01\pi$ mm mrad. The other lines show the expected functions for a 20% larger emittance by varying the inferred source size or divergence.

Because of the long plasma to vacuum transition (mm scale) at the exit of our gas cell, we discuss the effect this has on the electron beam envelope using an analytical model. While the beam is trapped and accelerated in the plasma wakefield, the strong linear focusing forces keep the beam size small and the normalized emittance remains constant. The evolution of the rms electron beam envelope, $x(s)$, in an ion channel (as in the plasma blow-out regime) neglecting space charge and acceleration is given by [26]

$$x(s)'' + k_\beta^2 x(s) - \varepsilon^2/x(s)^3 = 0. \quad (2)$$

Here k_β is the betatron wave number; in an ion channel $k_\beta = k_p/\sqrt{2\gamma}$ [27], where k_p is the plasma wave number which depends on the density of the background electrons, n_e. The dynamics of the beam envelope are therefore determined by the plasma density and the beam emittance. When the focusing force of the plasma balances the expansion due to the beam emittance, the beam envelope remains constant with a matched size $x_m = \sqrt{\varepsilon/k_\beta}$. For the parameters in our experiment the matched beam size is $x_m \lesssim 0.2$ μm and the betatron wavelength is $\sim$0.5 mm. Our emittance measurement method is not suitable to quantify changes in the beam size while it is still in the plasma. The expected scaling of the matched beam size with the plasma density $x_m \sim n_e^{-1/4}$ can thus not be validated. However, the discrepancy between the larger inferred source size from the emittance measurements above ($\lesssim 1$ μm) and the matched beam size in the plasma can be resolved by considering the density transition from the plasma to the vacuum. If the electron beam passes through a density downramp comparable to or longer than its betatron wavelength, the decreasing transverse focusing forces lead to an increase of the matched spot size and (due to the conserved emittance) to a decrease of the divergence [13]. This effect was investigated by solving Eq. (2) for a density downramp obtained from computational fluid dynamics (CFD) simulations [28] modeling the experiment (gas cell with a 1 mm exit hole diameter). The beam divergence obtained from the lens two position scan measurement (0.45 mrad) is reproduced if the density from the CFD simulations is attenuated smoothly to zero from $z \sim 10$ mm [Fig. 4(a)]. The need to truncate the density downramp to reproduce the experiment suggests that the model assumption of a pure ion channel is not valid for the entire downramp, probably due to laser diffraction and depletion. The downramp also causes a shift of the effective source position [as evident in Fig. 4(a)] which affects the retrieved emittance value. For this example the source position shift is approximately 8 mm and leads to a $\sim$14% smaller retrieved emittance. The fitted electron beam energy to this shifted electron beam source is $\sim$14 MeV below the expected beam energy from the measurement,

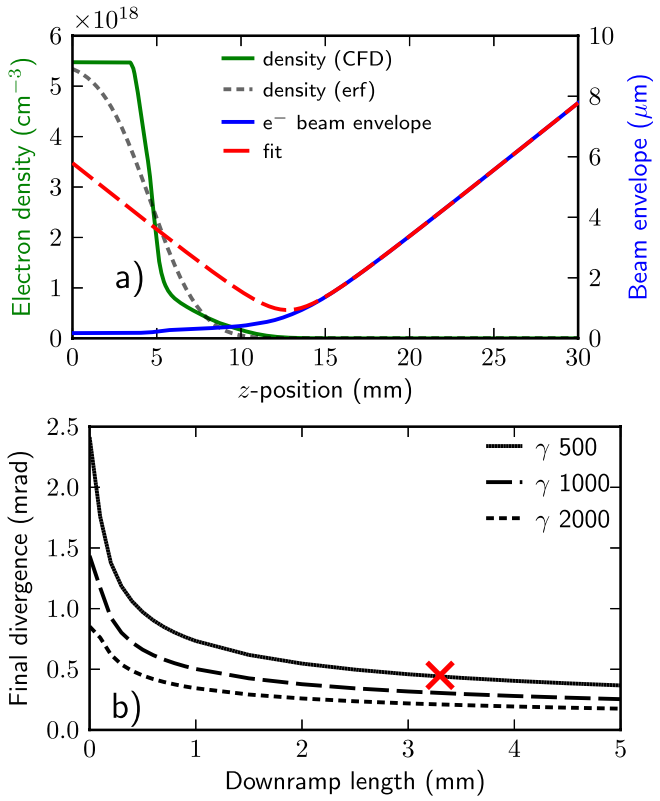

FIG. 4. Simulations of the electron beam envelope and final divergence after the density downramp at the exit of the accelerator. (a) Evolution of the electron beam envelope (solid blue) in the plasma to vacuum density transition (solid green, based on CFD simulations) according to Eq. (2). The fit line (red dashed) describes an effective electron source with the same emittance as the beam envelope but propagating without the focusing forces of the plasma; the beam waist and divergence are consistent with the values inferred from the lens position scan measurements. The same effective source is obtained with a downramp modeled by an error function of length 3.3 mm (black dotted). The physical exit of the gas cell is at $z = 5$ mm. (b) The final divergence after the accelerator downramp as a function of its length, l {where $n_e = n_0[0.5\mathrm{erf}(-z/l) + 1]$}, for three different beam energies with normalized emittances of 0.2π mm mrad. The cross indicates the case in (a).

which is beyond the reasonable experimental error for the measured energy (< 10 MeV). To resolve this discrepancy requires further analysis with empirical measurements of the density downramp (as shown in [29]) in place of the CFD simulations used here. The qualitative agreement of the model with the measurements suggests the possibility of a further reduction by using a longer downramp. Figure 4(b) shows that the majority of the divergence decrease occurs within the first few millimeters and is relatively insensitive to longer downramps. In [30], a smaller beam divergence was observed for larger diameter capillaries (and therefore longer density downramps at the exit). Aside from the differences in the laser propagation and electron injection in the different sized plasma channels, the longer downramp offers a further possible cause for the observed reduced divergence. To our knowledge the beam divergence presented here is the smallest published to date for LWFA beams and can be attributed to the longer density downramp of our gas cell as opposed to commonly used supersonic gas jets. To reduce the source divergence further, a separate density peak (in our case $\sim 10^{15}$ cm^{-3}) could be incorporated slightly downstream of the main downramp and be used to focus the beam similarly to work being done on plasma lenses [31]. Provided the laser pulse still contains enough energy to create an ion channel, this even promises to focus the entire bunch as opposed to only the rear part for a purely beam-driven plasma lens. The benefit of a smaller source divergence is the reduced bunch elongation for a given beam transport system [22].

In this paper we have demonstrated a spectrally resolved quadrupole scan measurement of the emittance of laser-wakefield-accelerated electrons. Two alternative methods, one employing a lens position scan, the other using a small energy bandwidth of a single shot, both give a normalized emittance of $\sim 0.2\pi$ mm mrad. This value stays constant with energy as expected from the linear focusing fields in the wakefield during acceleration. A simple model of the electron beam envelope evolution in the density transition from the plasma to the vacuum supports the measured data. The method is not limited by the field errors of the lenses nor by the space charge of typical LWFA electron beams. The measured emittance values intrinsically include the effect of the density downramp at the accelerator exit and therefore can be applied to subsequent applications. However, as our measurement is in the x plane, a larger emittance in the y plane in the direction of the laser polarization cannot be excluded (e.g., due to an interaction between the electrons and the laser beam in the wakefield [32]). A plasma accelerator relying on continuous self-injection will result in a correlation between longitudinal position within the beam and electron energy. The energy-resolved emittance measurements presented here therefore allow the measurement of the transverse slice emittance, an essential parameter for the design of a free-electron laser based on plasma accelerated electron beams.

ACKNOWLEDGMENTS

This work was funded by TR18, MAP (DFG), and EURATOM–IPP.

[1] T. Tajima and J. M. Dawson, Phys. Rev. Lett. **43**, 267 (1979).
[2] E. Esarey, C. Schroeder, and W. Leemans, Rev. Mod. Phys. **81**, 1229 (2009).
[3] C. G. R. Geddes, C. Toth, J. van Tilborg, E. Esarey, C. B. Schroeder, D. Bruhwiler, C. Nieter, J. Cary, W. P.

Leemans, and J. V. Tilborg, Nature (London) **431**, 538 (2004).
[4] S. P. D. Mangles, C. D. Murphy, Z. Najmudin, A. G. R. Thomas, J. L. Collier, A. E. Dangor, E. J. Divall, P. S. Foster, J. G. Gallacher, C. J. Hooker *et al.*, Nature (London) **431**, 535 (2004).
[5] J. Faure, Y. Glinec, A. Pukhov, S. Kiselev, S. Gordienko, E. Lefebvre, J. P. Rousseau, F. Burgy, and V. Malka, Nature (London) **431**, 541 (2004).
[6] W. P. Leemans, B. Nagler, a. J. Gonsalves, C. Toth, K. Nakamura, C. G. R. Geddes, E. Esarey, C. B. Schroeder, S. M. Hooker, and C. T_oth, Nat. Phys. **2**, 696 (2006).
[7] M. Fuchs, R. Weingartner, A. Popp, Z. Major, S. Becker, J. Osterho_, I. Cortrie, B. Zeitler, R. Hörlein, G. D. Tsakiris *et al.*, Nat. Phys. **5**, 826 (2009).
[8] S. Kneip, C. McGuffey, J. L. Martins, S. F. Martins, C. Bellei, V. Chvykov, F. Dollar, R. Fonseca, C. Huntington, G. Kalintchenko *et al.*, Nat. Phys. **6**, 980 (2010).
[9] F. Grüner, S. Becker, U. Schramm, T. Eichner, M. Fuchs, R. Weingartner, D. Habs, J. Meyer-ter Vehn, M. Geissler, M. Ferrario *et al.*, Appl. Phys. B **86**, 431 (2007).
[10] O. Lundh, J. Lim, C. Rechatin, L. Ammoura, A. BenIsmaïl, X. Davoine, G. Gallot, J.-P. Goddet, E. Lefebvre, V. Malka *et al.*, Nat. Phys. **7**, 219 (2011).
[11] A. Buck, M. Nicolai, K. Schmid, C. M. S. Sears, A. Sävert, J. M. Mikhailova, F. Krausz, M. C. Kaluza, and L. Veisz, Nat. Phys. **7**, 543 (2011).
[12] S. Fritzler, E. Lefebvre, V. Malka, F. Burgy, A. E. Dangor, K. Krushelnick, S. P. D. Mangles, Z. Najmudin, J.-P. Rousseau, and B. Walton, Phys. Rev. Lett. **92**, 165006 (2004).
[13] C. M. S. Sears, A. Buck, K. Schmid, J. Mikhailova, F. Krausz, and L. Veisz, Phys. Rev. ST Accel. Beams **13**, 92803 (2010).
[14] E. Brunetti, R. Shanks, G. Manahan, M. Islam, B. Ersfeld, M. Anania, S. Cipiccia, R. Issac, G. Raj, G. Vieux *et al.*, Phys. Rev. Lett. **105**, 3 (2010).
[15] N. Delerue *et al.*, in *Proceedings of the 23rd Particle Accelerator Conference, Vancouver, Canada, 2009* (IEEE, Piscataway, NJ, 2009), p. 3597.
[16] M. Schnell, A. Sävert, B. Landgraf, M. Reuter, M. Nicolai, O. Jäckel, C. Peth, T. Thiele, O. Jansen, A. Pukhov *et al.*, Phys. Rev. Lett. **108**, 075001 (2012).
[17] S. Corde, K. Phuoc, R. Fitour, J. Faure, and A. Tafzi, Phys. Rev. Lett. **107**, 255003 (2011).
[18] S. Kneip, C. McGuffey, J. Martins, M. Bloom, V. Chvykov, F. Dollar, R. Fonseca, S. Jolly, G. Kalintchenko, K. Krushelnick *et al.*, Phys. Rev. ST Accel. Beams **15**, 2 (2012).
[19] M. G. Minty and F. Zimmermann, *Measurement and Control of Charged Particle Beams* (Springer, New York, 2003).
[20] K. Wille, *The Physics of Particle Accelerators: An Introduction* (Oxford University Press, New York, 2000).
[21] A. Popp, Ph.D. thesis, LMU München, 2011.
[22] R. Weingartner, M. Fuchs, A. Popp, S. Raith, S. Becker, S. Chou, M. Heigoldt, J. Wenz, B. Zeitler, Z. Major *et al.*, Phys. Rev. ST Accel. Beams **14**, 052801 (2011).
[23] A. Lumpkin, B. Yang, W. Berg, M. White, J. Lewellen, and S. Milton, Nucl. Instrum. Methods Phys. Res., Sect. A **429**, 336 (1999).
[24] S. Becker, M. Bussmann, S. Raith, M. Fuchs, R. Weingartner, P. Kunz, W. Lauth, U. Schramm, M. El Ghazaly, F. Grüner *et al.*, Phys. Rev. ST Accel. Beams **12**, 102801 (2009).
[25] S. G. Anderson and J. B. Rosenzweig, Phys. Rev. ST Accel. Beams **5**, 1 (2002).
[26] M. Reiser, *Theory and Design of Charged Particle Beams* (Wiley-VCH, Berlin, 2008).
[27] E. Esarey, B. Shadwick, P. Catravas, and W. Leemans, Phys. Rev. E **65**, 1 (2002).
[28] OpenFoam, http://www.openfoam.prg
[29] T. Weineisen, B. Göppner, K. Schmid, M. Fuchs, H. Schröder, S. Karsch, and F. Grüner, Phys. Rev. ST Accel. Beams **14**, 1 (2011).
[30] K. Nakamura, B. Nagler, C. Toth, C. G. R. Geddes, C. B. Schroeder, E. Esarey, W. P. Leemans, A. J. Gonsalves, and S. M. Hooker, Phys. Plasmas **14**, 056708 (2007).
[31] M. C. Thompson, H. Badakov, J. B. Rosenzweig, G. Travish, N. Barov, P. Piot, R. Fliller, G. M. Kazakevich, J. Santucci, J. Li *et al.*, Phys. Plasmas **17**, 073105 (2010).
[32] S. Mangles, A. Thomas, M. Kaluza, O. Lundh, F. Lindau, A. Persson, F. Tsung, Z. Najmudin, W. Mori, C.-G. Wahlström *et al.*, Phys. Rev. Lett. **96**, 1 (2006).
[33] General Particle Tracer, http://www.pulsar.nl/gpt.